Table 1 Parameters β, γ, and b of gamma distributions for u and v wind component perturbation standard deviation σ

Wind component	β, s/m	γ	b, m/s
u	12.13	12.43	0.42
v	6.89	5.31	0.90

where β and γ are estimated from sample statistics of σ for each wind component and b is an empirically derived bias parameter that ensures the best fit to the observed distribution[7]:

$$\gamma = \left(\frac{\text{mean}(\sigma - b)}{\text{stdev}(\sigma - b)}\right)^2 \beta = \frac{\gamma}{\text{mean}(\sigma - b)} \tag{7}$$

The values for β, γ, and b are listed in Table 1. The theoretical cumulative gamma probability functions for wind component standard deviations (50–2000-m wavelength band) are derived by integration of Eq. (6) from a lower limit of zero to any desired value y for σ.

The simulated wind component perturbation profiles are adjusted such that the variation of component standard deviation as a function of altitude observed in the original sample of 518 high-pass filtered Jimsphere wind component profiles is reproduced in the simulated profiles.[7] To address a concern that the high-pass filtered wind component standard deviation illustrated can be unduly influenced at high altitudes by Jimsphere tracking system noise and data gaps, the standard deviations were also calculated from a sample of 26 high-resolution Automated Meteorological Profiling System (AMPS) wind profiles.[8] The AMPS wind measurement error is not sensitive to balloon azimuth and altitude because it is based on global positioning system tracking for determination of balloon position and calculation of wind vectors along the balloon trajectory. The standard deviations from this relatively small sample of AMPS profiles obtained during a five-month period exhibit the same behavior derived from the larger Jimsphere winter sample. The empirical function derived from the Jimsphere sample also fits the AMPS variation.[7]

The enhancement process is completed by adding a unique simulated wind component perturbation profile to each Rawinsonde wind component profile that has been cubic-spline interpolated to the same altitude interval (25 m) as the simulated profile.[7]

Summary

Detailed wind profiles that are statistically representative at a selected launch site are a critical requirement in design studies to establish vehicle structural integrity and program risk for vehicle operations within the range of detailed wind-profile variability. A methodology has been developed for simulation of wind-profile perturbations in a prescribed wavelength band. These perturbation profiles to wavelengths as small as tens of meters are appended to statistically representative low-resolution Rawinsonde wind-profile databases that are likely to be available at or near candidate launch sites. The simulation process is based on the inverse transform of the Fourier series having random components that define the PSD and the uniformly distributed phase angles of the Fourier harmonics. The PSD model for wind-profile perturbations is derived from a large sample (518) of Jimsphere detailed wind profiles. Profiles so derived are a reasonable choice for initial launch-vehicle design studies. Once a launch site is selected, it would be prudent to establish a wind-profile measurement program based on Jimsphere or its equivalent to obtain a statistically representative sample of detailed wind profiles. As the development process continues toward commitment to hardware production, the vehicle design originally based on enhanced Rawinsonde profiles could be assessed with the launch site high-resolution wind profiles.

Acknowledgment

This study was performed for the Marshall Space Flight Center under the Program Information Systems Mission Services Contract (NAS8-6000).

References

[1] Sako, B. H., Kim, M. C., Kabe, A. M., and Yeung, W. K., "Derivation of Atmospheric Gust-Forcing Functions for Launch-Vehicle Loads Analysis," *Journal of Spacecraft and Rockets*, Vol. 37, No. 4, 2000, pp. 434–442.

[2] Adelfang, S. I., Smith, O. E., and Batts, G. W., "Ascent Wind Model for Launch Vehicle Design," *Journal of Spacecraft and Rockets*, Vol. 31, No. 3, 1994, pp. 502–508.

[3] Fichtl, G. H., and Perlmutter, M., "Stochastic Model of Vertically Nonhomogeneous Gusts," *Journal of Spacecraft and Rockets*, Vol. 13, No. 10, 1976, pp. 577, 578.

[4] Wilfong, T. L., and Boyd, B. F., "Winds Aloft to Support Space and Missile Launches," *Proceedings of the Third International Conference on the Aviation Weather System*, American Meteorological Society, Boston, 1989, pp. 102–107.

[5] Wilfong, T. L., Smith, S. A., and Crosiar, C. L., "Characteristics of High Resolution Wind Profiles Derived from Radar Tracked Jimspheres and the Rose Processing Program," *Journal of Atmospheric and Oceanic Technology*, Vol. 14, No. 4, 1997, pp. 318–325.

[6] Johnson, D. (ed.), "Terrestrial Environment (Climatic) Criteria Handbook for Use in Aerospace Vehicle Development," NASA HDBK-1001, 11, Aug. 2000.

[7] Adelfang, S. I., "Simulation of Wind Profile Perturbations for Launch Vehicle Ascent Flight Systems Design Assessments," AIAA Paper 2003-0896, Jan. 2003.

[8] Wilfong, T. L., Maier, M. L., Crosiar, C. L., Hinson, M. S., and Divers, B., "Characteristics of Wind Profiles Derived from GPS Based Automated Meteorological Profiling System (AMPS)," Ninth Conf. on Aviation, Range and Aerospace Meteorology, Paper J8.2, American Meteorological Society, Boston, 2000.

C. Kluever
Associate Editor

Analytical Methods for Predicting Grain Regression in Tactical Solid-Rocket Motors

Roy Hartfield,* Rhonald Jenkins,* John Burkhalter,† and Winfred Foster†
Auburn University, Auburn, Alabama 36849-5338

Introduction

IN many practical solid-rocket-motor design efforts, final geometric designs for grains are arrived at using numerical layering techniques. This process is geometrically versatile and imminently practical for cases where small numbers of final geometries are considered. However, for a grain-design-optimization process where large numbers of grain configurations must be considered, the generation of grids for each candidate design is often prohibitive. For such optimization processes, analytical developments of burn perimeter and port area for two-dimensional grains are critically important.[1] Most modern rocket-propulsion texts do not provide geometric details for grain design.[2,3]

Analytical developments for solid-rocket-motor grains were much more prevalent in the decades before widespread use of microcomputers. A summary of one version of the burnback equations for the star grain and for part of one type of wagon wheel can be found

---

Received 17 June 2003; presented as Paper 2003-4506 at the AIAA/ASME/SAE/ASEE 39th Joint Propulsion Conference, Huntsville, AL, 20–23 July 2003; revision received 10 September 2003; accepted for publication 10 September 2003.

*Associate Professor, Aerospace Engineering Department. Member AIAA.

†Professor, Aerospace Engineering Department. Member AIAA.

in Barrere et al.[4] Analytical methods have also been developed for the truncated star and for the dendrite.[5] A more recent and comprehensive treatment of the topic was completed by Ricciardi for the star grain and for the truncated star.[6] Other potential grain configurations are described with few details in NASA publications.[7,8] The treatment of the star grain by Ricciardi includes tapered grains and both convex and concave star points with analysis for every phase of burning.

Star grains, which can be modeled using Ricciardi's equation set, are common in booster motors; however, many tactical missiles employ wagon-wheel grains and derivatives of wagon-wheel grains. This Note expands on the work of Ricciardi by presenting the development of analytical methods for these grains.

Long-Spoke Wagon Wheels

Wagon-wheel grain designs can include "spokes" of only one type or spokes of two or more types. Wagon wheels with two different sizes of spokes are commonly referred to as dendrites. If the spokes burn out from the sides, the designs are referred to herein as "long-spoke wagon wheels." Wagon wheels in which the spokes burn out from the ends are referred to as "short-spoke" designs. Figure 1 shows a sample of three different possible types of wagon wheels. The first is a typical long-spoke wagon wheel, the second is a wagon wheel configured as a dog bone, and the third is a dendrite.

The long-spoke wagon wheel designs have been developed and included in one form in Barrere et al.[4] Those results are summarized as follows. To provide a lucid presentation of the wagon-wheel geometry, a diagram showing the basic wagon-wheel layout is included as Fig. 2. The star-grain geometry needs only six parameters for a complete definition of the grain cross section. The wagon-wheel grain requires the seven parameters shown in the diagram. In the development of all of the relationships presented herein, the burning of the grain is considered to be spatially uniform and it is assumed that the regression of the grain is normal to the burning surface.

The wagon-wheel geometry is more restrictive than the star geometry because the spokes must not be allowed to overlap. If the angle δ is defined as the angle between the central axis of the spoke and the edge of the shoulder of the spoke, the relationship defining $\tan(\delta)$ can be written as

$$\tan\delta = \frac{R_p \sin(\pi\varepsilon/N) - f}{R_i + f/\sin(\theta/2) + H_{y=0}/\tan(\theta/2)} \tag{1}$$

where H is defined by

$$H = R_p \sin(\pi\varepsilon/N) - y - f \tag{2}$$

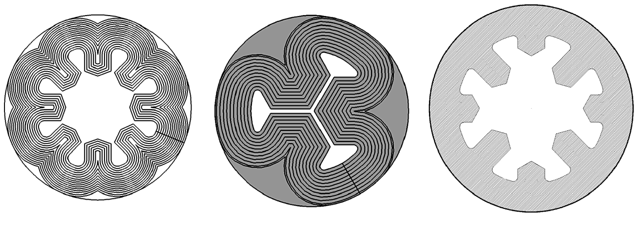

Fig. 1 Wagon-wheel designs: long-spoke, dog-bone, and dendrite.

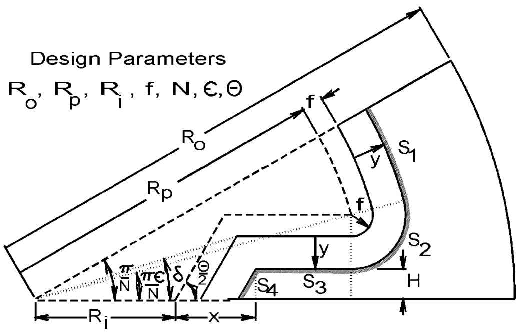

Fig. 2 Long-spoke wagon-wheel geometry.

With these definitions, it is clear that δ of less than π/N prevents spoke overlap.

The burn perimeter is constructed from two arcs and two line segments as

$$S = 2N \times \left[(R_p + f + y)\left(\frac{\pi}{N} - \frac{\pi\varepsilon}{N}\right) + (y+f)\left(\frac{\pi}{2} + \frac{\pi\varepsilon}{N}\right) + R_p \cos\frac{\pi\varepsilon}{N} - R_i - \frac{y+f}{\sin(\theta/2)} + \frac{H}{\tan(\theta/2)} + \frac{H}{\sin(\theta/2)} \right] \tag{3}$$

The port area for phase 1 burning can be constructed from two arcs and a right triangle with the trapezoidal spoke area subtracted off:

$$A_p = 2N \times \left\{ \left[\frac{(R_p + f + y)^2}{2}\left(\frac{\pi}{N} - \frac{\pi\varepsilon}{N}\right) + \frac{(f+y)^2}{2}\left(\frac{\pi}{2} + \frac{\pi\varepsilon}{N}\right) \right] + \frac{R_p^2}{2}\sin\left(\frac{\pi\varepsilon}{N}\right)\cos\left(\frac{\pi\varepsilon}{N}\right) - \left\{ H\left[R_p\cos\frac{\pi\varepsilon}{N} - R_i - \frac{y+f}{\sin(\theta/2)} + \frac{H}{\tan(\theta/2)} \right] + \frac{1}{2}\frac{H^2}{\tan(\theta/2)} \right\} \right\} \tag{4}$$

Phase 2 burning occurs when the spoke burns out ($H = 0$), in which case

$$y \geq R_p \sin(\pi\varepsilon/N) - f \tag{5}$$

For phase 2, the expression for the arc S_1 is unchanged and both segments S_3 and S_4 are zero. S_2 is an arc of radius $y + f$ and an increasingly smaller angle ϕ. ϕ and the burn perimeter can be expressed as

$$\phi = \frac{\pi}{2} + \frac{\pi\varepsilon}{N} - \cos^{-1}\left[\frac{R_p \sin(\pi\varepsilon/N)}{y+f}\right] \tag{6}$$

$$S = 2N\left[(R_p + f + y)\left(\frac{\pi}{N} - \frac{\pi\varepsilon}{N}\right) + (y+f)\phi \right] \tag{7}$$

The port area for phase 2 is written as the sum of two arc sections and a triangle:

$$A_p = N \times \left\{ (R_p + f + y)^2\left(\frac{\pi}{N} - \frac{\pi\varepsilon}{N}\right) + (f+y)^2\left\{\frac{\pi}{2} + \frac{\pi\varepsilon}{N} - \cos^{-1}\left[\frac{R_p\sin(\pi\varepsilon/N)}{y+f}\right]\right\} + R_p \sin\left(\frac{\pi\varepsilon}{N}\right)\left(R_p\cos\left(\frac{\pi\varepsilon}{N}\right) + (y+f) \times \sin\left\{\cos^{-1}\left[\frac{R_p\sin(\pi\varepsilon/N)}{y+f}\right]\right\}\right) \right\} \tag{8}$$

Phase 2 ends when the burning first reaches the case, that is, when

$$R_p + f + y > R_o \tag{9}$$

Final-Phase Burning

The area remaining after the wall has been reached by the burning surface S_1 can be labeled as phase 3 burning for the long-spoke wagon wheel. The equations for that mode of burning are not well

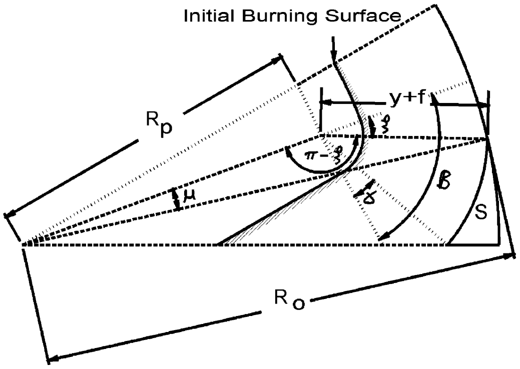

Fig. 3 Final-phase burning.

developed in the literature and some attention is paid to that development here. Figure 3 is a schematic diagram showing one method for analyzing this segment of the burn.

Using straightforward trigonometry, the angles β and γ can be represented as

$$\beta = \left(\frac{\pi}{2} - \frac{\theta}{2} + \frac{\pi\varepsilon}{N}\right) \tag{10}$$

$$\gamma = \tan^{-1}\left[\frac{\sqrt{(y+f)^2 - R_p \sin(\pi\varepsilon/N)^2}}{R_p \sin(\pi\varepsilon/N)}\right] - \frac{\theta}{2} \tag{11}$$

Using the law of cosines, ξ can be determined as follows:

$$\xi = \pi - \cos^{-1}\left[-\frac{R_o^2 - R_p^2 - (y+f)^2)}{2R_p(y+f)}\right] \tag{12}$$

The burn perimeter, a section of an arc, becomes

$$S = 2N[(y+f)(\beta - \gamma - \xi)] \tag{13}$$

The maximum burn distance that can occur can be arrived at using the diagrams in Figs. 1 and 3 and may be expressed as

$$y_{\max} = \sqrt{[R_o - R_p\cos(\pi\varepsilon/N)] + [R_p\sin(\pi\varepsilon/N)]} - f \tag{14}$$

A convenient method for determining the port area for this phase is to add an arc of angle μ, the arc section corresponding to the burning segment, and a triangle through angle $\pi\varepsilon/N$ and then subtract a triangle through angle μ. The angle μ must be determined first and may be written, using the law of sines, as

$$\mu = \sin^{-1}\{[(y+f)/R_o]\sin(\pi - \xi)\} \tag{15}$$

Collecting the areas then results in an expression for the port area:

$$A_p = N \times \left\{\begin{array}{l} R_o^2[(\pi/N)(1-\varepsilon) + \mu] + (y+f)^2(\beta - \gamma - \xi) \\ +R_p\sin(\pi\varepsilon/N)\big[R_p\cos(\pi\varepsilon/N) \\ \quad + \sqrt{(y+f)^2 - R_p\sin(\pi\varepsilon/N)^2}\,\big] \\ -R_p\sin(\mu)\big[R_p\cos(\mu) + \sqrt{(y+f)^2 - R_p\sin(\mu)^2}\,\big] \end{array}\right\} \tag{16}$$

Short-Spoke Wagon Wheel

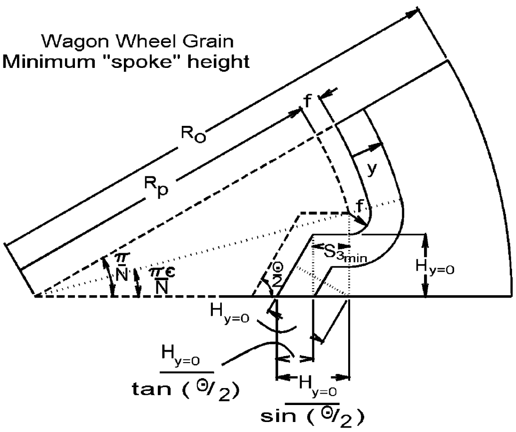

Fig. 4 Short-spoke wagon wheel.

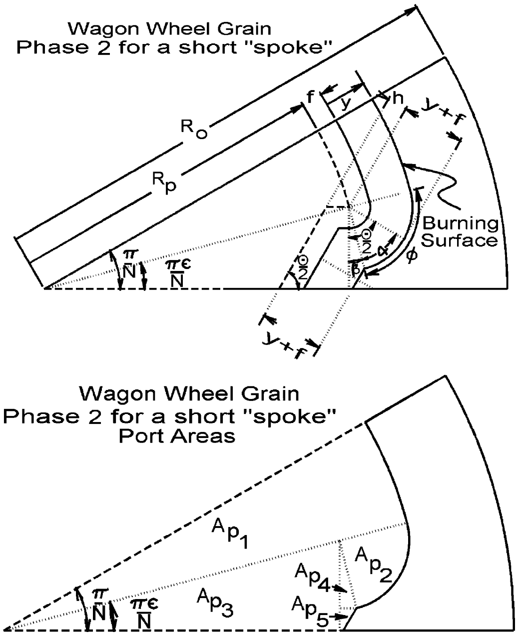

Fig. 5 Short-spoke wagon wheel, phase 2.

The short-spoke wagon-wheel geometry has not previously been developed in the literature. The geometric determination regarding whether the spoke burns out from the sides or from the end can be made with the aid of the diagram in Fig. 4. For the spoke to burn out from the sides, it must have a minimum height. This effectively limits the value of the burn-perimeter segment S_3, as shown in Fig. 4. At the transition from long spoke to short spoke, an expression based on the horizontal length from the center of the grain to the center of the burning arc can be written as

$$R_p\cos\left(\frac{\pi\varepsilon}{N}\right) = R_i + \frac{f + H_{y=0}}{\sin(\theta/2)} = R_i + \frac{R_p\sin(\pi\varepsilon/N)}{\sin(\theta/2)} \tag{17}$$

For application of the long-spoke development, the following requirement must be met:

$$R_p\cos\left(\frac{\pi\varepsilon}{N}\right) - R_i - \frac{R_p\sin(\pi\varepsilon/N)}{\sin(\theta/2)} \geq 0 \tag{18}$$

Otherwise, the wagon wheel is of the short-spoke type.

If S_3 is below the minimum allowable length for the long-spoke analysis, the parameters for phase 1 can be calculated exactly as for the long spoke except that phase 1 will end when S_3 goes to zero. A phase 2 burn will then occur as depicted in Fig. 5. In this phase, S_1 is an arc as predicted earlier, S_2 is an arc of radius $y + f$ and angle ϕ,

S_3 is zero, and S_4 is the remaining slanted face. Phase 2 will begin for a burn distance of

$$\mathrm{web1} = \left[R_p \cos\left(\frac{\pi\varepsilon}{N}\right) - R_i - \frac{f}{\sin(\theta/2)} - \frac{R_p \sin(\pi\varepsilon/N) - f}{\tan(\theta/2)}\right] \tan\left(\frac{\pi - \theta/2}{2}\right) \tag{19}$$

The analysis of this phase is dependent on h, which can be represented by

$$h = \left[R_p \cos\left(\frac{\pi\varepsilon}{N}\right) - \frac{R_p \sin(\pi\varepsilon/N)}{\tan(\theta/2)} - R_i\right] \sin\left(\frac{\theta}{2}\right) \tag{20}$$

α can then be calculated as follows. From Fig. 5, it is clear that

$$\alpha = \cos^{-1}[1 - h/(y + f)] \tag{21}$$

The angles are related to each other as follows:

$$\beta = \theta/2 - \alpha \tag{22}$$

$$\phi = \pi/2 + \pi\varepsilon/N - \beta \tag{23}$$

The length S_2 can now be written as

$$s_2 = (y + f)\phi \tag{24}$$

To obtain an expression for S_4, the β triangle can be analyzed to produce

$$s_4 = [R_p \sin(\pi\varepsilon/n) - (y + f)\cos(\beta)]/\sin(\theta/2) \tag{25}$$

Finally, the burn perimeter for phase 2 of a short-spoke wagon wheel is

$$S = 2N(S_1 + S_2 + S_4) \tag{26}$$

The port areas for phase 2 can be assembled as shown in Fig. 5.

The areas A_{p_1}, A_{p_2}, and A_{p_3} are arcs and triangles that can be written as

$$A_{p_1} = \tfrac{1}{2}(R_p + f + y)^2(\pi/N - \pi\varepsilon/N) \tag{27}$$

$$A_{p_2} = \tfrac{1}{2}(y + f)^2\phi \tag{28}$$

$$A_{p_3} = \tfrac{1}{2}R_p^2 \sin(\pi\varepsilon/N)\cos(\pi\varepsilon/N) \tag{29}$$

The area A_{p_4} is a triangle of area

$$A_{p_4} = \tfrac{1}{2}(y + f)^2 \cos\beta \sin\beta \tag{30}$$

For the most general case, A_{p_5} should be constructed as a trapezoid as follows:

$$A_{p_5} = [R_p \sin(\pi\varepsilon/N) - (y + f)\cos\beta][(y + f)\sin\beta] - \tfrac{1}{2}S_4^2 \sin(\theta/2)\cos(\theta/2) \tag{31}$$

The total port area for a short-spoke phase 2 burn can then be represented as

$$A_p = 2N(A_{p_1} + A_{p_2} + A_{p_3} + A_{p_4} + A_{p_5}) \tag{32}$$

For this type of wagon wheel, phase 2 will end when S_4 goes to zero, provided that the outer radius is large enough. This condition for going to phase 3 would be

$$y = \frac{R_p \sin(\pi\varepsilon/N)}{\cos\beta} - f \tag{33}$$

A closed-form solution for the web thickness for phase 2 can be developed. At the end of phase 2, the following condition exists:

$$(y + f)^2 = [R_p \sin(\pi\varepsilon/N)]^2 + \{R_i + [y + f/\sin(\theta/2)] - R_p \cos(\pi\varepsilon/N)\}^2 \tag{34}$$

This equation can be rearranged and written as a quadratic in $y + f$

$$\{[1/\sin(\theta/2)]^2 - 1\}(y + f)^2 + \{2[R_i - R_p \cos(\pi\varepsilon/N)]/\sin(\theta/2)\} \times (y + f) + \left\{[R_p \sin(\pi\varepsilon/N)]^2 + [R_i - R_p \cos(\pi\varepsilon/N)]^2\right\} = 0 \tag{35}$$

The root using the negative term in the quadratic equation provides the physically appropriate solution for $y_{\text{end phase II}} + f$. The web thickness for phase 2 is then

$$\mathrm{web2} = (y_{\text{end phase II}} + f) - f - \mathrm{web1} \tag{36}$$

Phase 3 for this configuration can be analyzed like phase 2 for the long spoke and the final phase is the same as the final phase for the long spoke. It should be noted that if h is negative, the geometry is overconstrained. Such geometries can be represented by the star-grain geometry if the $\theta/2$ parameter is dropped and the six remaining parameters are specified. Both geometries can be represented with the same seven parameters if it is clear that the grain will be a star if h is calculated to be negative.

Summary

Algebraic expressions such as those included in this Note represent the foundation of fast analysis for cylindrically perforated solid-rocket-motor grains and combinations of grains. It should be noted that all of the grains mentioned in this Note, except the dendrite, could be represented by the same seven parameters, to be adjusted by any optimization scheme, thereby allowing a tremendous variety of cylindrically perforated grains. If care is taken to maintain a constant web thickness in tapered grains, the equations presented in this Note can be used to model tapered grains accurately, provided that linear averages of geometrically similar cross sections are taken between the two ends of the grain. The versatility and speed with which grain geometries can be explored using this more classical approach to grain design allow the parameter space for motor design to be explored efficiently by design-optimization algorithms.

References

[1] Anderson, M., Burkhalter, J., and Jenkins, R., “Design of a Guided Missile Interceptor Using a Genetic Algorithm,” *Journal of Spacecraft and Rockets*, Vol. 38, No. 1, 2001, pp. 28–35.

[2] Davenas, A., *Solid Rocket Propulsion Technology*, Pergamon, Oxford, 1993.

[3] Sutton, G., and Biblarz, O., *Rocket Propulsion Elements*, 7th ed., Wiley, New York, 2001.

[4] Barrere, M., Jaumotte, A., Veubeke, B., and Vandenkerckhove, J., *Rocket Propulsion*, Elsevier, Amsterdam, 1960.

[5] Sforzini, R. H., “Notes on Solid-Propellant Rocket Motors Including Jet Propulsion Fundamentals,” Aerospace Engineering Dept., Auburn Univ., Auburn, IL, May 1980.

[6] Ricciandi, A., “Generalized Geometric Analysis of Right Circular Cylindrical Star Perforated and Tapered Grains,” *Journal of Propulsion and Power*, Vol. 8, No. 1, 1992, pp. 51–58.

[7] “Solid Propellant Grain Design and Internal Ballistics,” NASA SP 8076, URL: http://library.msfc.nasa.gov/cgi-bin/lsp8000 [cited 1 June 2003].

[8] “Solid Rocket Motor Performance Analysis and Prediction,” NASA SP 8039, URL: http://library.msfc.nasa.gov/cgi-bin/lsp8000 [cited 1 June 2003].

T. Lin
Associate Editor